Phase diagram of the frustrated spin-$\frac{1}{2}$ Heisenberg antiferromagnet with cyclic-exchange interaction

Andrey Chubukov* and Eduardo Gagliano
Physics Department and Materials Research Laboratory, University of Illinois at Urbana-Champaign, Urbana, Illinois 61801

Carlos Balseiro
Instituto Balsiero and Centro Atomico Bariloche, 8400 San Carlos de Bariloche, Rio Negro, Argentina
(Received 13 November 1991)

We study the effect of four-spin cyclic-exchange interactions on the magnetic properties of the spin-$\frac{1}{2}$ Heisenberg antiferromagnetic on a two-dimensional square lattice with the two-spin interactions between nearest and next-nearest neighbors. We found that the four-spin exchange competes with the effects of frustration and this competition leads to a very rich phase diagram. We use the standard spin-wave formalism, the perturbative expansions around various dimerized states and finite-cluster calculations to study the locations of different phases of the model. The phase diagram in the frustration-cyclic exchange plane involves two collinear phases [(π,π) and $(0,\pi)$], three canted states, and two different dimerized configurations.

I. INTRODUCTION

A large number of experiments have shown that the proximity to a magnetic transition plays an important role in the normal and superconducting properties of the high-T_c cuprate oxide materials.[1] The electronic structure of the insulating phase of these compounds has been investigated[2] and found to have a charge-transfer gap 1.4–2.0 eV depending on the material, which varies linearly with the Madelung potential.[3] Although the insulating gap is not of the Mott-Hubbard type, it has been shown recently,[4] by identifying the *valence* (mainly O_{2p}) and the Cu_{3d} *conduction* bands of the CuO planes as the *lower* and *upper* Hubbard bands, respectively, that the one-band Hubbard model with the intermediate coupling $U/t \approx 8-10$ can mimic well the electronic structure of the oxides at the low-energy scales.

The one-band Hubbard model has been applied to interpret photoemission,[5] optical conductivity,[6] and x-ray absorption experiments.[7] It reproduces qualitatively such experimentally measured properties of the high-T_c compounds as the presence of the mid-infrared peak in the spectral weight, a slow variation of the total spectral weight with the hole doping concentration, and the presence of the Drude peak whose intensity grows with the doping.[6]

At half-filling and at large U/t, the magnetic properties of the Hubbard model can be described by the effective spin Hamiltonian whose leading term is known to be the antiferromagnetic Heisenberg interaction between nearest neighbors. However, other exchange interactions, namely, the Heisenberg exchange with further neighbors and the four-spin cyclic exchange, are also known to be present in the effective spin Hamiltonian[8] and for intermediate $U/t \approx 8-10$ are by no means negligible in comparison with the leading term. On the other hand, for the more realistic multiband Hamiltonians[9] with one hole per Cu atom and large U_d/t_{pd}, a perturbative expansion in t_{pd}/V_{pd} and t_{pd}/Δ, where V_{pd} is the Coulomb repulsion between neighboring Cu and O atoms, $\Delta = E_p - E_d$ is the charge-transfer energy, and t_{pd} is the hopping parameter, produces an effective spin Hamiltonian with the dominant contribution coming from four-spin cyclic-exchange interactions.[10] Small-cluster calculations for multiband models show that away from the perturbative region the four-spin exchange probably does not survive as the leading term but still gives a significant contribution to the effective spin model.[11] Thus, for $E_p - E_d = 1.2$ eV, the effective exchange parameters have been estimated as $J_1 = 0.69$ eV, $J_2 = 0.17$ eV, and $K = 0.52$ eV, where J_1, J_2, and K measure the strength of the nearest, next-nearest, and four-spin couplings, respectively.[12] Even though the numerical results may be influenced by finite-size effects, their predictions are important for the real materials. In fact, a second peak recently observed in the Raman spectrum in the insulating phase of the high-T_c cuprates has been identified as due to large four-spins cyclic-exchange interaction between the Cu spins.[13]

In this paper we study the influence of the four-spin exchange interaction on the magnetic properties of the 2D square lattice Heisenberg antiferromagnet. The Hamiltonian we consider involves the exchange interaction between first, second, and third nearest neighbors and also four-spin exchange interaction between spin operators along the elementary square plaquette. In the explicit form,

$$\mathcal{H} = \mathcal{H}_J + \mathcal{H}_K , \tag{1}$$

where

$$\mathcal{H}_J = \sum_{\mathbf{i}} \sum_{n=1,2,3} J_n \mathbf{S}_{\mathbf{i}} \cdot \mathbf{S}_{\mathbf{i}+\hat{\delta}_n} \tag{1'}$$

and

$$\mathcal{H}_{\mathcal{K}}=2K\sum_i (\mathbf{S}_i\cdot\mathbf{S}_{i+\hat{\mathbf{x}}})(\mathbf{S}_{i+\hat{\mathbf{y}}}\cdot\mathbf{S}_{i+\hat{\mathbf{x}}+\hat{\mathbf{y}}}) + (\mathbf{S}_i\cdot\mathbf{S}_{i+\hat{\mathbf{y}}})(\mathbf{S}_{i+\hat{\mathbf{x}}}\cdot\mathbf{S}_{i+\hat{\mathbf{x}}+\hat{\mathbf{y}}}) - (\mathbf{S}_i\cdot\mathbf{S}_{i+\hat{\mathbf{x}}+\hat{\mathbf{y}}})(\mathbf{S}_{i+\hat{\mathbf{y}}}\cdot\mathbf{S}_{i+\hat{\mathbf{x}}}) \ . \quad (1'')$$

Here $\hat{\boldsymbol{\delta}}=(\hat{\mathbf{x}},\hat{\mathbf{y}})$ denotes unit vectors in both directions of a square lattice, $\hat{\boldsymbol{\delta}}_2$ and $\hat{\boldsymbol{\delta}}_3$ measure the distance between a given spin and his second and third near neighbors, respectively, and $\mathbf{S}_i$ are spin-$\frac{1}{2}$ operators.

In the strong-coupling limit of the Hubbard model, the exchange parameters are given by $J_1=4t^2/U-24t^4/U^3$, $J_2=J_3=4t^4/U^3$, and $K=40t^4/U^3$. For arbitrary t/U as well as for a finite doping, the constraint on the values of the couplings is relaxed and both K and J_n must be considered as independent parameters.[14]

Since the discovery of high-T_c superconductivity, the so-called J_1-J_2-J_3 model with $\mathcal{H}=\mathcal{H}_J$ has been at the heart of the discussion of the magnetic properties of the cuprates.[15–19] The pure Heisenberg limit is well understood. Perturbative (spin waves), numerical, and self-consistent (for example, Schwinger boson) approaches all agree that (1) the ground state has *long-range order* and (2) quantum fluctuations are *strong enough* to reduce the staggered magnetization M_1 from its classical value to 0.31.[20]

The J_1-J_2 model has also been analyzed using different techniques. All these studies agree that the phase diagram should involve three phases.[15–19] Two of them are ordered with the ordering momenta (π,π) at small J_2 and $(0,\pi)$ at large J_2, while the third phase is magnetically disordered and emerges around the classical transition point $J_2=J_1/2$ due to quantum fluctuations. There have been several suggestions about the type of the ground state in this phase but recent studies strongly favor the columnar dimer state as the most plausible candidate for the ground state in the intermediate region.[15–19] With nonzero J_3, the phase diagram involves also two incommensurate phases with the momenta (π,Q) and (Q,Q) and a disordered intermediate phase near the boundary between any of these phases and the (π,π) ordered state.[21]

Little is known about the magnetic phases induced by the four-spin interactions. Some time ago, multiple-spin interactions have been considered as the possible candidate to account for ferromagnetism in solid ^{3}He, and the theoretical predictions for the 2D triangular lattice[22] turned out to be consistent with the experiments on the layers of solid ^{3}He absorbed on Grafoil.[23]

In this work, we study the influence of the four-spin exchange on the magnetic phase diagram of the 2D square lattice frustrated Heisenberg antiferromagnet. For simplicity, we restrict our calculations to the case $J_3=0$. The remainder of the paper is organized as follows. In Sec. II, we discuss the phase diagram of Eq. (1) first in the quasiclassical (large-S) approximation and then by using a special bosonization technique for $S=\frac{1}{2}$. In Sec. III we present the results of finite-cluster calculations. Finally, Sec. IV is devoted to the summary and conclusions.

II. PHASE DIAGRAM

In this section we describe the phase diagram of Eq. (1) in the parametric space $(J_2/J_1,K/J_1)$. We start with the discussion of a quasiclassical (large-S) phase diagram which follows from the standard spin-wave calculations and then discuss how it should be modified in case of $S=\frac{1}{2}$.

A. Quasiclassical phase diagram

Let us start with a standard spin-wave formalism which allows one to determine the boundaries of different phases in the large-S limit. Since the four-spin term contains additional overall factor of S^2, it is convenient to redefine the corresponding coupling and measure the strength of the four-spin interactions in terms of $\tilde{K}=KS^2$. Let us first discuss what happens when J_2 is zero. For small enough $\tilde{K}$, the ground state obviously has the long-range Néel order. Small deviations from the Néel state are well described by the bosonic excitations (spin waves). A standard procedure of linking spin operators with bosons via, say, Dyson-Maleev transformation together with a diagonalization of the quadratic form in Bose operators results in a usual spin-wave spectrum

$$\varepsilon_k=\sqrt{A_k^2-B_k^2} \ , \quad (2)$$

where

$$A_k=J_1-4\tilde{K}+2\tilde{K}(1-\nu_x\nu_y) \ , \qquad B_k=(J_1-4\tilde{K})\frac{\nu_x+\nu_y}{2} \ , \quad (2')$$

and $\nu_i=\cos k_i$. It immediately follows from Eq. (2) that the Néel phase is at least locally stable for all $\tilde{K}$ less than the critical value $\tilde{K}=J_1/4$. At $\tilde{K}=J_1/4$, the spin-wave velocity softens to zero and the spin-wave excitations have quadratic dispersion both near $k=0$ and $k=(\pi,\pi)$. The fact that the softening involves only the special points in the Brilloin zone clearly indicates that the destruction of the Néel order at $\tilde{K}=J_1/4$ occurs via a continuous second-order phase transition. This transition is a rather peculiar one since naively one might expect that the softening of the spin-wave excitations in the vicinity of the quasiclassical transition line $\tilde{K}=J_1/4$ will result in the logarithmical divergence of quantum fluctuations which, in turn, will lead to a finite strip of the paramagnetic phase around $\tilde{K}=J_1/4$ no matter how large the spin S is. This scenario is known to be valid for the J_1-J_2-J_3 model.[21,24] However, in the present case, the analogous softening of the spin-wave excitations is accompanied by the decrease in the strength of the zero-point fluctuations measured by the anomalous coupling B_k. As follows from Eq. (2'), this coupling tends to zero as $\tilde{K}$ approaches the critical point and quantum fluctuations *do not diverge*.

The absence of the zero-point motion at $\tilde{K}=J_1/4$ means that at this point, the fluctuations of the spins from two different ferromagnetically ordered sublattices in the Néel phase decouple from each other (the spectrum at $\tilde{K}=J_1/4$ is exactly the same as in the Heisenberg *fer-*

romagnet with the interaction only along the diagonals). As an obvious consequence, the ferromagnetic ordering within each sublattice survives also for $\tilde{K} > J_1/4$, but the angle θ between the two sublattices shifts from its value in the Néel phase ($\theta=0$). The resulting canted configuration is shown in Fig. 1. The value of θ is determined by the minimization of the classical ground-state energy per spin:

$$E(\theta)=E_{\text{Néel}}+\frac{NS^2}{4\tilde{K}}[(4\tilde{K}\cos\theta-J_1)^2-(4\tilde{K}-J_1)^2] , \quad (3)$$

where

$$E_{\text{Néel}}=(-2J_1+2\tilde{K})NS^2 .$$

The minimization with respect to θ yields

$$\cos\theta=-\frac{J_1}{4\tilde{K}} . \quad (3')$$

In contrast to what is known about the Néel phase, the canted configuration as in Fig. 1 has a nonzero net magnetization $M_z \sim (1-\cos\theta)=1-J_1/4\tilde{K}$ and $M_{x,y} \sim |\sin\theta| \sim (1-J_1/4\tilde{K})^{1/2}$, that is the canted spin ordering completely breaks down SO(3) spin symmetry. Consequently, the low-energy theory for this phase should contain three massless branches of bosonic excitations. This is what one has in conventional helical spin structures. A peculiarity of the present case is that the system has a nonzero *net* magnetization and the bosonic modes related to the fluctuations of the vector part of the SO(3) order parameter (i.e., of the unit vector on the S_2 sphere) are mixed to produce a single gapless excitation with quadratic dispersion.

The spin-wave dispersion relation can be easily obtained by using a bosonization procedure referenced to the canted state. After making a transformation to a reduced zone scheme and diagonalizing the quadratic in bosons part of the Hamiltonian, we obtain

$$\varepsilon_k^1=J_1(1-\nu_x\nu_y)^{1/2}\left[2\cos^2\theta\left[1-\frac{\nu_x+\nu_y}{2}\right]-\cos(2\theta)(1-\nu_x)(1-\nu_y)\right]^{1/2} , \quad (4a)$$

$$\varepsilon_k^2=J_1(1-\nu_x\nu_y)^{1/2}\left[2\cos^2\theta\left[1+\frac{\nu_x+\nu_y}{2}\right]-\cos(2\theta)(1+\nu_x)(1+\nu_y)\right]^{1/2} \quad (4b)$$

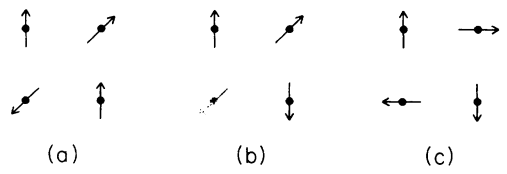

FIG. 1. Canted spin configurations. (a) With ferromagnetic ordering along diagonals. (b) With antiferromagnetic ordering along diagonals. (c) Orthogonal configuration.

In accordance with the general arguments, ϵ_k^1 scales as k^2 at $k \approx 0$ while ϵ_k^2 is linear in k at low momenta. Also, the excitations described by ϵ_k^1 and ϵ_k^2 are real for arbitrary θ, and so the canted phase with continuously varying θ will survive at least as a local minimum for *all* $\tilde{K} > J_1/4$.

Now we turn to nonzero J_2. First, at $\tilde{K}=0$, the Néel (π,π) phase is known to be stable up to $J_2 \approx J_1/2$ when the system undergoes a first-order transition into the $(\pi,0)$ or $(0,\pi)$ state.[24,25] The width of the hysteresis region scales as $\frac{\ln S}{S}$ for $S \gg 1$. The situation is most likely to be different for $S=\frac{1}{2}$ when instead of the first-order transition between two ordered phases, the system passes through the intermediate magnetically disordered dimerized state with a spontaneously broken symmetry of translations by one site. We will discuss the $S=\frac{1}{2}$ case in more detail below and now will continue with the quasiclassical phase diagram. For $J_2 > J_1/2$, the $(\pi,0)$ phase is known to exhibit the "order from disorder" phenomena,[26] i.e., the excitations above this state contain extra zero modes which are not related to any kind of broken symmetry, but signal that the classical ground state is infinitely degenerate. For a particular case of J_1-J_2 model, this degeneracy manifests itself in that for arbitrary $J_2 > J_1/2$, a homogeneous rotation of the spins from one of the magnetic sublattices formed by the second neighbors about the direction of the spins from the other sublattice does not cost energy provided one preserves the antiferromagnetic ordering within each sublattice. This "accidental degeneracy" is known to be lifted by quantum fluctuations which produce a correction to the ground-state energy[27]

$$\delta E_{\text{quant}} \sim J_1 NS^2\left[-\frac{1}{S}\cos^2\theta\right] , \quad (5)$$

which depends on the angle θ between the antiferromagnetic sublattices and, according to Eq. (5), stabilizes the configurations with $\theta=0$ or π, i.e., $(\pi,0)$ or $(0,\pi)$ phases.

Four-spin exchange interaction also removes the accidental degeneracy $J_2 > J_1/2$, already for classical spins. However, the corresponding θ-dependent correction to the ground-state energy has a different sign with respect to that in Eq. (5),

$$\delta E = 4\tilde{K}NS^2\cos^2\theta , \quad (6)$$

and thus the four-spin exchange interactions *compete* with the quantum effects and favor the $(\pi/2,\pi/2)$ configuration where the spins from different sublattices are arranged orthogonal to each other. It immediately follows from this simple analysis that for $\tilde{K} \sim J_1/S$ the system will undergo a transition from $(0,\pi)$ to $(\pi/2,\pi/2)$ phase. In the leading order in $1/S$, this transition is of first order. However, with the next-order corrections in $1/S$ it may become a continuous one via an intermediate phase when the angle between the sublattices continuously varies from 0 to $\pi/2$.

All the other transitions occur at $J_2 < J_1/2$. First, the calculations of the spin-wave spectrum above the Néel state generalized to a finite J_2 show that the canting of

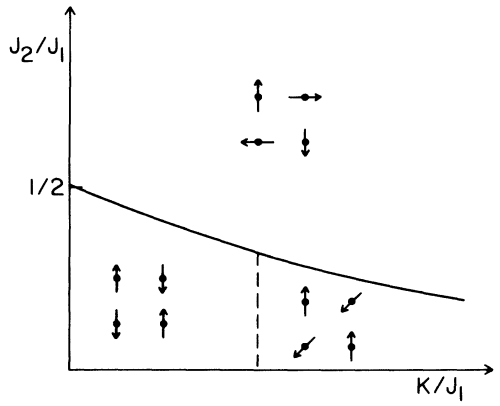

FIG. 2. Quasiclassical phase diagram of the J_1-J_2-K model.

the spin structure starts at $\tilde{K}=J_1/4$ independently of the value of J_2. Second, the simple analysis based on the comparison of the classical ground-state energies shows that when the J_2 coupling increases along $\tilde{K}<J_1/4$ and reaches the value of

$$J_2=\frac{J_1}{2}-\tilde{K}\ , \tag{7}$$

the system undergoes a first-order transition into the $(\pi/2,\pi/2)$ state. The same happens for $\tilde{K}>J_1/4$, but now the critical value of J_2 is inverse proportional to the four-spin coupling:

$$J_2=\frac{J_1}{16\tilde{K}}\ . \tag{8}$$

The resulting quasiclassical phase diagram is presented in Fig. 2.

B. The phase diagram for $S=\frac{1}{2}$

Obviously, the results obtained in the large-S limit do not necessary correctly reproduce the phase diagram in the more realistic case of $S=\frac{1}{2}$ where the effects of quantum fluctuations are by no means small. The most striking consequence of the large quantum fluctuations is the possibility for new magnetically disordered phases to appear on the phase diagram, especially in the vicinity of the quasiclassical phase boundaries where the softening of the spin-wave excitations gives rise to an additional enhancement of quantum fluctuations. For J_1-J_2 model this is exactly the situation one has in the vicinity of the classical transition point $J_2=J_1/2$, where both numerical and analytical calculations show that for $S=\frac{1}{2}$ the transition between the two states with long-range magnetic order [i.e., (π,π) and $(0,\pi)$ states] occurs via the intermediate magnetically disordered *dimerized* phase. This is to be contrasted with the first-order between the (π,π) and $(0,\pi)$ states found for large S.

Among different dimer configurations, the most favorable candidates for the ground state are the so-called columnar and staggered dimers [Figs 3(a) and 3(b)]. In the mean-field approximation, when one neglects the interaction between different dimers, both configurations have the same energy, $E=-\frac{3}{8}NJ_1$, at $J_2=J_1/2$. However, quantum corrections were shown to break this degeneracy and to favor energetically the columnar dimer: in the Hartree-Fock approximation, the gain in the energy due to quantum fluctuations is $\Delta E=J_1(3/\pi)(1-2/\pi)$.[18]

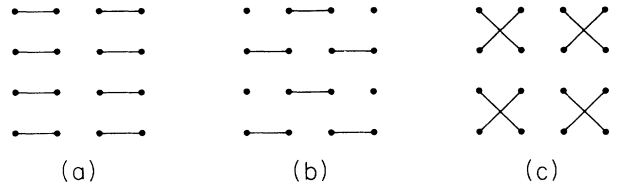

FIG. 3. Various dimerized configurations. (a) columnar, (b) staggered, (c) diagonal.

Also, the analysis based on the bosonization technique developed to study the excitations above a dimerized ground state[17,18,28] shows that while at the quadratic order in bosons the columnar dimer is stable only at a single particular ratio of the couplings $J_2=J_1/2$, the interaction between the bosonic excitations stabilizes the dimerized phase in a finite region around $J_2=J_1/2$.[17,18] This is another peculiar example of the "order from disorder" phenomena since if the columnar dimer were stable only at a single ratio of the couplings, its excitation spectrum would have the entire lines of zero modes in the Brillouin zone and quantum corrections would be logarithmically divergent in two dimensions.

The nonzero four-spin exchange interaction changes the situation. For the ground state made by the columnar dimers, a half of the elementary plaquettes contains two pairs of spins which are involved in the dimer configurations. As a result, the cyclic exchange influences the ground-state energy already in the mean-field approximation and, for positive K, increases the energy by the amount $\delta E_c=\frac{9}{16}NK$. On the other hand, the staggered dimer configuration contains exactly one dimer per elementary plaquette and its mean-field energy does not depend on $\tilde{K}$. Hence, the four-spin cyclic interaction favors energetically the staggered dimer and thus again competes with the quantum effects in the system and induces a first-order transition between the columnar and staggered dimer configurations. If the Hartree-Fock approximation is used to account for the quantum fluctuations, the transition occur at $K=K_c=0.61J_1$.

Our next aim is to find a stability region of the staggered dimer in the presence of the cyclic exchange. To do this, we calculate the excitations above the dimerized ground state and determine the region in the parametrical space where they are real, i.e., where the staggered dimer is at least a local minimum. A way to perform these calculations is to use the bosonization technique referred to the dimerized state.[28] Specifically, if $\vec{S}_1$ and $\vec{S}_2$ are two neighboring spins to be involved in a dimer, then we introduce the ferro- and antiferromagnetic vectors:

$$\vec{M}=\vec{S}_1+\vec{S}_2 \quad \text{and} \quad \vec{L}=\vec{S}_1-\vec{S}_2\ . \tag{9}$$

The dimer (singlet) state is defined by $M=0$ $[\vec{M}^2=M(M+1)]$. We introduce now three bosons a, b, c

with canonical commutation relations in the following manner:

$$M^z=a^\dagger a-b^\dagger b\ ,$$
$$M^+=\sqrt{2}(a^\dagger c-c^\dagger b)\ , \tag{10}$$
$$M^-=\sqrt{2}(c^\dagger a-b^\dagger c)\ ,$$
$$L^z=-(c^\dagger U+Uc)\ ,$$
$$L^+=\sqrt{2}(a^\dagger U+Ub)\ , \tag{11}$$
$$L^-=\sqrt{2}(b^\dagger U+Ua)\ ,$$

where $U=(1-a^\dagger a-b^\dagger b-c^\dagger c)^{1/2}$. The physical subspace is obtained by considering states with at most one boson. The bosonic vacuum $a|0\rangle=b|0\rangle=0$ is the singlet $M=0$ state and the triplet states $M=1$ are the states with one excited boson a, b, or c. In this physical subspace, we have the correct commutation relations:

$$[M_i,M_j]=i\epsilon_{ijk}M_k\ ,$$
$$[L_i,L_j]=i\epsilon_{ijk}M_k\ , \tag{12}$$
$$[M_i,L_j]=i\epsilon_{ijk}L_k\ ,$$

together with the constraint $S^2=\frac{3}{4}$. Moreover, the matrix elements of transitions between physical and nonphysical states are zero. The bosonization scheme given by (11) and (12) may thus be regarded as an exact at zero temperature. It is completely analogous to the Holstein-Primakoff expression for the spin operators in the case of $S=\frac{1}{2}$; the only difference is in the form of the vacuum state. The transformation (11) and (12) can be generalized to spin S leading to $(2S+1)^2-1$ coupled bosons, allowing one to study the systems with higher spin.[29]

Equations (11) and (12) can be applied to each pair of spins which form a separate dimer and this maps the original $S=\frac{1}{2}$ problem onto the Bose gas. Since both Heisenberg and four-spin cyclic exchange interactions involve the spins which may belong to different dimers, the bosons are allowed to hop. The hopping leads to a dispersion of the excitations and also to zero-point fluctuations, which give rise to the interactions between bosons and destroy the perfect dimer ordering.

In the present study we will calculate the spectrum in the "spin-wave" approximation, i.e., by restricting with only the terms which are quadratic in bosons. Strictly speaking, this approximation is uncontrolled since the problem has no small parameter which could play the role of $1/S$ and ensure the smallness of the anharmonic effects. However, for nonzero K, the staggered dimer turns out to be stable in a *finite* region in the parametrical space. In view of this, it seems very unlikely that anharmonic terms can produce any qualitative rather than quantitative change to our results.

The calculations are quite straightforward and after the transformation to bosons obviously require Fourier transformation to a momentum space and the diagonalization of the quadratic form in bosons. Working along these lines, we obtain three degenerate branches of the quasiparticles excitations as it should be since the ground state is a spin singlet. The energies of the quasiparticles are given by

$$\varepsilon_k=J_1^{1/2}[J_1(1-\nu_{2x})+2(J_1-2J_2)\nu_x\nu_y+\tfrac{3}{2}K\nu_{2x}]^{1/2}\ . \tag{13}$$

In writing Eq. (13), we supposed that the dimers are directed along the x axis.

For $K=0$, the excitations given by Eq. (13) are real only at the single particular ratio of the couplings, $J_2=J_1/2$. However, for nonzero K, ϵ_k is real in a finite region of the J_2 coupling. A simple analysis of Eq. (13) shows that the stability region first increases with K, reaches a maximum at $K=8J_1/9$, and then falls down and disappears at $K=4J_1/3$. The explicit boundaries of the staggered dimer are given by

$$|J_1-2J_2|=\tfrac{3}{4}K,\quad K<\tfrac{8}{9}J_1\ ;$$
$$|J_1-2J_2|=\sqrt{(\tfrac{3}{2}K-J_1)(4J_1-3K)},\quad \tfrac{8}{9}J_1<K<\tfrac{4}{3}J_1\ . \tag{14}$$

As follows from Eq. (14), for $K<8J_1/9$, the instability of the dimer configuration occurs at $k_x=0$ and $k_y=0$ or π depending on whether J_1-2J_2 is positive or negative, correspondingly. Noticing that the expressions for the two neighboring spins which form a separate dimer read

$$\vec{S}_1=\tfrac{1}{2}(\vec{M}+\vec{L}),\quad \vec{S}_2=\tfrac{1}{2}(\vec{M}-\vec{L})\ , \tag{15}$$

and that only $\vec{L}$ has the contributions which are linear in Bose operators, we conclude that below the instability the system should condense into the (π,π) Néel state for $2J_2<J_1$ and into the $(\pi,0)$ state for $2J_2>J_1$. This agrees with the results of the quasiclassical description which as most of the investigations now agree should be valid not very close to $J_2=J_1/2$ even if the spin $S=\frac{1}{2}$.

On the other hand , for $8J_1/9<K<4J_1/3$, the instability of the dimerized state leads to the condensation of the single-particle excitations with some intermediate $k_x=\pm k_0$, where $k_0=\cos^{-1}[(4J_1-3K)/(6K-4J_1)]$ varies with K from $k_0=0$ at $K=8J_1/9$ to $k_0=\pi/2$ at $K=4J_1/3$. This clearly indicates that the transition occurs into the intermediate phase of the type already found in the quasiclassical description. We did not perform the calculations below the instability and thus cannot prove that the k_0 dependence of the condensate wave function ensures the transition into exactly the same intermediate state as was found for small J_2 in the quasiclassical approach [this would require $\mathrm{Im}\,A_{k_0}/\mathrm{Re}\,A_{k_0}=\tan k_0$, where $A_{k_0}=\langle(c_{k_0}+c^\dagger_{-k_0})\rangle$], but this is what one can expect on the general grounds since there are no reasons to believe that the quasiclassical theory fails far from $J_2=J_1/2$ even if $S=\frac{1}{2}$. Note that the critical value of K where the canting begins, $K_c=8J_1/9$, is very close to that found in the quasiclassical description and continued to $S=\frac{1}{2}$: $K_c=4\tilde{K}=J_1$. It is also remarkable that in the present description the intermediate phases exist on both sides from $J_2=J_1/2$ and hence not only the (π,π) but also the $(\pi,0)$ state transforms into the $(\pi/2,\pi/2)$ configuration at large K via the intermediate phase, where the now-antiferromagnetic or-

dering along each of the diagonals survives, but the angle between the antiferromagnetically ordered sublattices formed by the second neighbors shifts from 0 and varies continuously with K until it reaches the values of $\pi/2$ at $K=4J_1/3$.

In order to find the actual ground state for large values of K, we have compared the energy of the magnetically ordered $(\pi/2,\pi/2)$ configuration which meets the ground state in the quasiclassical approximation

$$E_{(\pi/2,\pi/2)}=-\frac{N}{2}\left[J_2+\frac{K}{4}\right], \tag{16}$$

with the mean-field energies of various dimerized configurations. Though the results obtained by this method are less conclusive than those based on the spin-wave approach, they unambiguously indicate that the $(\pi/2,\pi/2)$ state survives the competition with dimerized configurations for all values of $K>4J_1/3$. For example, one of the most plausible dimer configurations one might assume to exist at large K is that of Fig. 3(c) with the dimers directed along the diagonals of the square lattice. However, the mean-field energy of this state,

$$E_{XX}=-\frac{3}{8}N\left[J_2+\frac{K}{4}\right], \tag{17}$$

is larger than $E_{(\pi/2,\pi/2)}$ for all values of K.

The resulting phase diagram for the $S=\frac{1}{2}$ model is presented in Fig. 4. In analyzing this figure, we would like to make several comments. First, the tetracritical point $(J_2=J_1/2,K=4J_1/3)$ found in the spin-wave approach is most likely to be unstable against higher-order corrections and we expect it to decouple into the two tricritical points as is actually shown in Fig. 4. Second, the region near the phase boundaries between the dimerized and various magnetically ordered phases should be considered more carefully since the symmetries which are broken in these phases are completely different from each other. In the present approach, we found that the dimerized phase is separated from the phases with long-range magnetic order by the "disorder lines" where neither the continuous spin-rotation symmetry nor the discrete symmetry of translations by one side are broken. Since this is not what one can expect from the general arguments, we expect that either the transition will remain of the first order but will acquire a finite hysteresis width, or there will be a paramagnetic phase separating the staggered dimer from the states with the broken continuous symmetry.

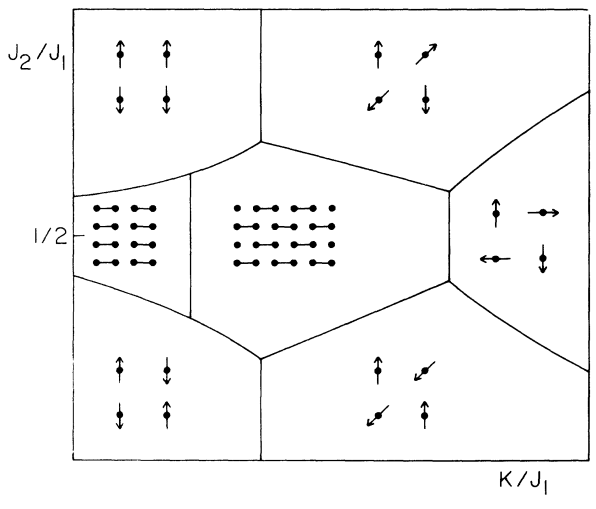

FIG. 4. The schematical phase diagram of the J_1-J_2-K model for $S=\frac{1}{2}$. The dimerized and canted spin configurations are the same as in Figs. 1 and 3.

It is also worth mentioning that the large-J_2 region of the phase diagram is only tentative since the only indication to the existence of the intermediate canted phase for $J_2>J_1$ comes from the calculation of the momenta of the instability in the staggered dimer phase. The direct calculations are different to perform because of the accidental degeneracy which violates the standard perturbative expansion about the $(\pi,0)$ state.

III. FINITE-CLUSTER CALCULATIONS

In this section we report the results of the exact diagonalization of the J_1-J_2-K model. We use a modified Lanczos[30] algorithm and calculate the low-energy levels as well as the mean values of the selected operators. Our purpose here is to do an *ab initio* searching of the phases found in Sec. II.

One key aspect of the study of magnetic properties on finite clusters is an appropriate choice of their size and geometry. For example, to allow the Néel (π,π) antiferromagnetic ordering, tilted square clusters must be constructed with the number of sites N given by $N=n^2+m^2$, where n and m are integer numbers satisfying the constraint $n+m=$even. This requirement is satisfied for clusters with $N=4,8,10,16,18,\ldots$.

The numerical study of the frustrated J_1-J_2 model imposed further restrictions on the cluster size. The point is that only the systems with $N/4$ even allow to avoid a frustration within a sublattice and to obtain a smooth scaling with the size of the system. These considerations reduce the sequence to clusters with $N=4,8,16,\ldots$ sites. Finally, the four-spin interaction involves square plaquettes, and we thus restricted to $N=4$, i.e., (2×2) and $N=16$, i.e., (4×4) systems with periodic boundary conditions.

The four-sites cluster can be solved analytically. The results are presented in Fig. 5. Three different phases can be detected in the parametrical space. Two of them (A and B) are spin singlets, while the large-K phase corresponds to $S=1$. The thermodynamic analogs of the spin-singlet phases can be found immediately since the first excited states in the A and B phases are the (π,π) or $(0,\pi)$ triplets, respectively. Obviously, in the thermodynamic limit these phases should coincide with the (π,π) and $(0,\pi)$ ordered states. On the other hand, at this level of consideration, it is hard to draw definite conclusions about the thermodynamic limit of the $S=1$ phase. For larger clusters, we expect to find a better agreement with the theoretical phase diagram of Sec. II. However, the simple calculation for the 2×2 cluster al-

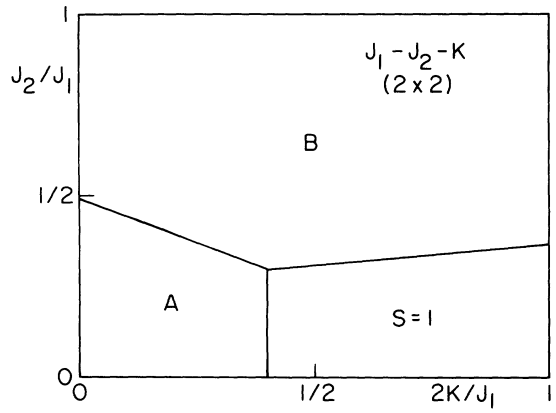

FIG. 5. Phase diagram of the J_1-J_2-K model on the 2×2 cluster for $S=\frac{1}{2}$. Depending on the values of J_2/J_1 and K/J_1, the ground state is either $S=0$ singlet (A or B) with $E_A=-4J_1+2J_2+13K/2$ and $E_B=-6J_2-3K/2$, or $S=1$ triplet with $E=-2J_1+2J_2-7K/2$.

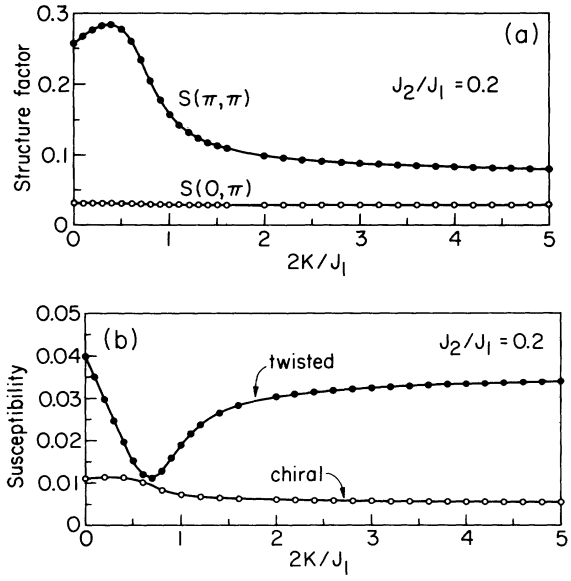

FIG. 6. Plots of (a) the structure factors $S(\pi,\pi)$ and $S(0,\pi)$ and (b) the twist (●) and chiral (○) susceptibilities as functions of K/J_1 for $J_2/J_1=0.20$.

ready teaches us several things. First, for $K=0$, the level crossing between two singlet states occurs at the same ratio of the couplings, $J_2/J_1=\frac{1}{2}$, as in the classical description. This clearly points out that for larger clusters it should be possible to detect the intermediate disordered phase around this point. Second, for $J_2=0$, the 2×2 analog of the Néel phase loses its stability at $2K_c/J_1=\frac{2}{5}$, which is noticeably smaller than the corresponding value found in Sec. II. Finally, the third point to mention is that for large J_2, the region of the $(0,\pi)$ phase stretches up to large values of K ($K_c=4J_2-J_1$) in complete contradiction with the quasiclassical results which make the $(0,\pi)$ phase unfavorable already for very small K. Hence, even for larger clusters, we should expect the (π,π) Néel phase to lose stability at smaller K and the $(0,\pi)$ phase to survive up to higher values of K than those predicted in Sec. II.

A convenient way to study different phases as function of K and J_2 is to consider the static structure factor,

$$S(\vec{q})=\frac{1}{N^2}\sum_{l,m} e^{i\vec{q}\cdot(\vec{l}-\vec{m})}\langle \vec{S}_l\cdot\vec{S}_m\rangle$$

at $\vec{q}=(\pi,\pi)$ and $\vec{q}=(0,\pi)$. A simple insight why these momenta are important can be given by the quasiclassical calculations of $S(\vec{q})$ for a single plaquette. Indeed, for the Néel phase, $S(\pi,\pi)$ is larger than $S(0,\pi)$. When the angle between the two ferromagnetically ordered sublattices shifts from zero, $S(\pi,\pi)$ diminishes while $S(0,\pi)$ remains unchanged. In the orthogonal phase, both structure factors have classically the same value. In the $(0,\pi)$ phase the situation is reversible: The static structure factor $S(0,\pi)$ dominates over $S(\pi,\pi)$. Upon cantening, $S(0,\pi)$ diminishes while $S(\pi,\pi)$ remains unchanged.

We have studied different phases by making scans over K/J_1 for different values of J_2/J_1. The results for $J_2/J_1=0.20$ are presented in Figs. 6(a) and 6(b). Our results for the structure factors [Fig. 6(a)] clearly show that for $2K/J_1<0.5$, $S(\pi,\pi)$ is nearly a constant and has a value typical for a Néel phase. Between $0.50<2K/J_1<2.0$, $S(\pi,\pi)$ monotonically decreases while $S(0,\pi)$ remains unchanged. The strong reduction of the Néel order above the critical value of K, with $S(0,\pi)$ practically unchanged, signals that at these values of K the Néel phase is substituted by the intermediate canted spin configuration. At least, for larger values of the cyclic exchange, $2K/J_1>2$, both structure factors do not depend on K. Consequently, for all $2K/J_1>2$, the system is in a unique phase which is most likely to be an orthogonal one. The calculated difference between the values of $S(\pi,\pi)$ and $S(0,\pi)$ is presumably attributed to the effects of quantum fluctuations. An additional proof that the phase diagram for small J_2 involves three different phases comes from the calculations of the uniform twisted susceptibility $\langle \mathcal{O}_{\rm tw}^2\rangle$ where

$$\vec{\mathcal{O}}_{\rm tw}=\frac{1}{N}\sum_{\rm i}\vec{\mathcal{O}}_{\rm i} \tag{18}$$

and

$$\vec{\mathcal{O}}_{\rm i}=\tfrac{1}{2}(\mathbf{S}_{\rm i}\times\mathbf{S}_{\rm i+\hat{x}}+\mathbf{S}_{\rm i-\hat{x}}\times\mathbf{S}_{\rm i}+\mathbf{S}_{\rm i}\times\mathbf{S}_{\rm i+\hat{y}}+\mathbf{S}_{\rm i-\hat{y}}\times\mathbf{S}_{\rm i})\ .$$

Strictly speaking, for classical planar arrangement, this susceptibility should be equal to zero. However, out-of-plane fluctuations given rise to nonzero $\langle \mathcal{O}_{\rm tw}^2\rangle$ which indeed measures the cantening of the spin structure. Since the ground state is a spin singlet, without loss of generality, we can restrict our study to $\langle \mathcal{O}_z^2\rangle$. From Fig. 6(b), we see that the uniform twist susceptibility is nearly linearly enhanced between $2K/J_1=0.6$ and $2K/J_1=2$ and saturates for larger values of K. This is exactly what one should expect from the analysis given above. For completeness, in Fig. 6(b), we have also presented the data for the uniform chiral susceptibility, $\langle \mathcal{O}_{\rm ch}^2\rangle$, defined by

$$\mathcal{O}_{ch}=\frac{1}{N}\sum_i \mathcal{O}_i \tag{19}$$

and

$$\mathcal{O}_i=\mathbf{S}_i\cdot\mathbf{S}_{i+\hat{x}}\times\mathbf{S}_{i+\hat{y}}\ .$$

As in the pure J_1-J_2 model,[15,16] the chiral susceptibility shows no enhancement for any value of K.

For large values of J_2/J_1, we expect that the scanning over K/J_1 will allow us to detect also the dimerized states on the phase diagram. Figure 7 shows our results for $J_2/J_1=0.40$. For small and large values of the cyclic exchange, we recovered the same behavior as was observed for smaller values of J_2, namely (π,π) antiferromagnetic ordering for $2K/J_1<0.40$ and orthogonal phase for $2K/J_1>2.0$. However, the behavior at intermediate K is completely different. First, near $2K/J_1=0.5$, both structure factors quickly move towards each other, presumably indicating the existence of a tiny region of the intermediate disordered phase close to the antiferromagnetic instability. Starting from $2K/J_1=0.60$, both structure factors have practically the same values up to $2K/J_1\sim 1.6$. A previous experience in studying different phases in the pure J_1-J_2 model teaches us that the phase where both structure factors have equal values is most likely to be a dimerized one.[16] Keeping this in mind, we have also calculated the spin-spin correlation functions and indeed found that for intermediate K, the correlations are mostly restricted to the nearest neighbors as it should be for the dimerized configurations.

Our next aim is to investigate whether the system actually undergoes a transition between different dimer configurations as is predicted by the phase diagram of Fig. 4. To study this possibility, we calculated the susceptibilities for the two most plausible candidates for the ground state close to $J_2/J_1\sim 0.5$, namely, columnar and staggered dimers. These susceptibilities are defined by $\langle \mathcal{O}_{ud}^2\rangle$ and $\langle \mathcal{O}_{sd}^2\rangle$, where[19]

$$\mathcal{O}_{ud}=\frac{1}{N}\sum_i \mathcal{O}_i^{ud}$$

and

$$\mathcal{O}_i^{ud}=\tfrac{1}{2}[(-1)^{i_x}\mathbf{S}_i\cdot\mathbf{S}_{i+\hat{x}}-(-1)^{i_x}\mathbf{S}_i\cdot\mathbf{S}_{i-\hat{x}} +i(-1)^{i_y}\mathbf{S}_i\cdot\mathbf{S}_{i+\hat{y}}-i(-1)^{i_y}\mathbf{S}_i\cdot\mathbf{S}_{i-\hat{y}}]\ , \tag{20}$$

for the columnar dimer and

$$\mathcal{O}_{sd}=\frac{1}{N}\sum_i (-1)^{i_x+i_y}\mathcal{O}_i^{sd}\ ,$$

where

$$\mathcal{O}_i^{sd}=\tfrac{1}{2}(\mathbf{S}_i\cdot\mathbf{S}_{i+\hat{x}}-\mathbf{S}_i\cdot\mathbf{S}_{i-\hat{x}}+i\mathbf{S}_i\cdot\mathbf{S}_{i+\hat{y}}-i\mathbf{S}_i\cdot\mathbf{S}_{i-\hat{y}})\ ,$$

for the staggered dimer. In Fig. 8(b), we show both susceptibilities at $J_2/J_1=0.5$. From the corresponding calculations of the static structure factors, we expect the dimerized phase to be the ground state for $0<2K/J_1<2$. As it is clearly seen from Fig. 8, at small $2K/J_1$, the columnar dimer is definitely a preferable candidate for the ground state, while near the other boundary (as well as for larger K) the susceptibility of the staggered dimer is larger than that for the columnar one. This can be considered as the evidence in favor of the transition between different dimerized configurations at some intermediate $2K/J_1$. Well inside the dimerized phase both susceptibilities are nearly equal and it is hard to distinguish which dimerized state is preferable. The existence of the "hysteresis" behavior is partly attributed to the finite size of the system but also is the obvious consequence of the fact that in the real strongly fluctuating system, neither of the pure dimerized configurations from Sec. II actually answer to the ground state. The true ground state is always a mixture of different dimers and we can only point which configuration is preferable for a particular value of $2K/J_1$. Note, however, that the susceptibility of the staggered dimer continues to grow also in the region where the calculations of the static structure factors favor the orthogonal spin configuration. Presumably, this indicates that the actual transition between the staggered dimer and the orthogonal phase is rather smooth and the staggered correlations actually survive up to relatively large K.

At $J_2/J_1=0.60$, the scanning over K/J_1 (Fig. 9) allows us to detect one more phase on the phase diagram but also reveals some differences between analytical and numerical calculations. Namely, for very small K, the structure factors have nearly equal values, which again indicates that the system is in the dimer phase.[16] The calculation of the dimer susceptibilities clearly shows that

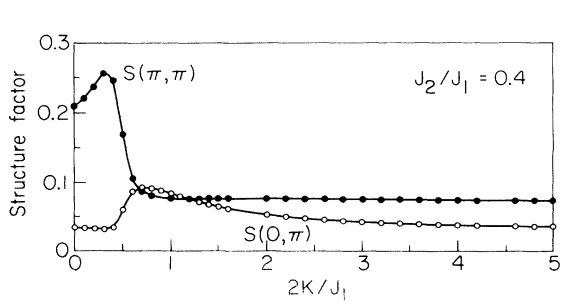

FIG. 7. Static structure factors $S(\pi,\pi)$ (●) and $S(0,\pi)$ (○) as functions of K/J_1 for $J_2/J_1=0.40$.

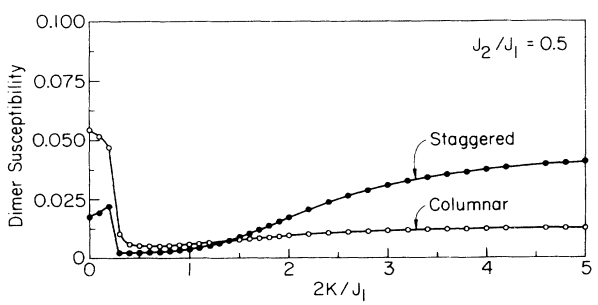

FIG. 8. The susceptibilities of the columnar (○) and staggered (●) dimers as functions of K/J_1 for $J_2/J_1=0.50$.

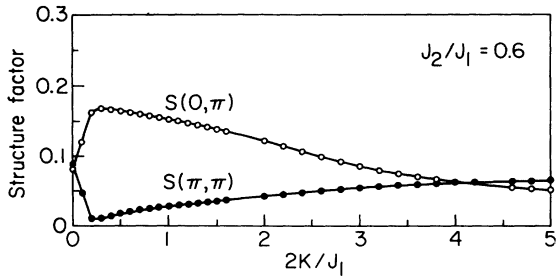

FIG. 9. The same as in Fig. 7, except that $J_2/J_1=0.60$.

for $K\approx 0$ the columnar susceptibility dominates over the staggered one, but quickly diminishes as K increases. This is consistent with the fact that the structure factors at (π,π) and $(0,\pi)$ also move apart with the increase in K. Starting from $2K/J_1=0.25$, $S(0,\pi)$ continuously decreases and nearly saturates at $2K/J_1$ larger than 4.5. This strongly suggests that above $2K/J_1=0.25$ the system is in the intermediate canted phase which transforms into the orthogonal one somewhere near $2K/J_1=4.5$. The fact that the intermediate phase stretches up to much larger K than one would expect from the analytical consideration is not surprising in view of the exact solution of the 2×2 cluster where this feature was already observed. What is, however, more unexpected, is the gradual increase of $S(\pi,\pi)$ between $2K/J_1=0.25$ and $2K/J_1=4.5$. We recall that, from the classical analysis, $S(\pi,\pi)$ should be a constant if the intermediate phase preserves the antiferromagnetic ordering along diagonals. It is hard to judge whether this difference is attributed to quantum fluctuations or the intermediate phase for $J_2/J_1>0.50$ has a more complicated structure than the simple canted configuration formed by two antiferromagnetically ordered sublattices [Fig. 1(b)].

The last scan was taken for $J_2/J_1=0.80$ (Fig. 10). Besides the broad intermediate phase already found in the previous figure, one can also determine the region of the ordered $(0,\pi)$ phase with nearly constant $S(0,\pi)$. Note that this phase stretches up to $2K/J_1=0.75$, i.e., to nearly the same value of the cyclic exchange as the (π,π) phase for small J_2/J_1. Also, with the chosen upper limit for K, namely $2K/J_1=5$, we cannot detect the transition to the orthogonal state, but the tendency towards this transition is clearly seen in Fig 10.

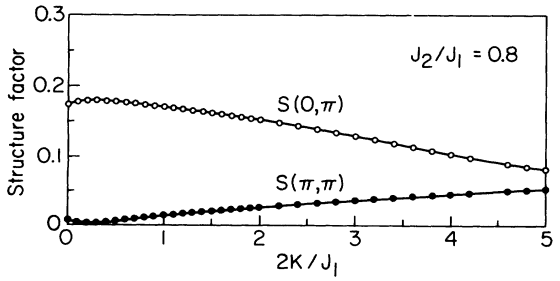

FIG. 10. Static structure factors $S(\pi,\pi)$ (●) and $S(0,\pi)$ (○) as functions of K/J_1 for $J_2/J_1=0.80$.

IV. SUMMARY AND CONCLUSIONS

In this paper, we presented the results of the analytical and numerical investigations of the phase diagram of the 2D square lattice Heisenberg antiferromagnet in the presence of next-nearest-neighbor coupling and the four-spin cyclic-exchange interactions. Several investigations of the strong-coupling limit of the Hubbard model as well as of the more realistic multiband Hamiltonians strongly suggest that both the further-neighbors Heisenberg exchange and the four-spin cyclic interaction between Cu spins should be taken into account in order to understand the nature of the magnetic ordering in the copper oxide superconductors.

We found that four-spin cyclic exchange competes with the frustration effects imposed by the further-neighbor exchange and this competition leads to a very rich phase diagram. For simplicity, we restricted our calculations to the case where Heisenberg interactions act only between nearest and next-nearest neighbors (J_1-J_2 model). We found that when the four-cycling exchange increases, both magnetically ordered phases of the J_1-J_2 model [the (π,π) for $J_2/J_1<\frac{1}{2}$ and the $(0,\pi)$ for $J_2/J_1>\frac{1}{2}$] first transform into intermediate canted phases and then to the unique configuration which we refer to as the orthogonal one, where the spins are aligned antiferromagnetically along diagonals and form the $\pi/2$ twist along both x and y directions.

Close to $J_2/J_1=\frac{1}{2}$, the ground state at $K=0$ is known to be a columnar dimer. We found that the four-spin cyclic exchange competes with the quantum fluctuations which favor the columnar dimer over the other dimer configurations. As a result, a nonzero K gives rise to a phase transition between the columnar dimer and the staggered one favored by the cyclic exchange.

The general phase diagram for the J_1-J_2-K model was found analytically in Sec. II and is presented in Fig. 4. Altogether, it contains seven phases. All these phases were found also in the numerical calculations of Sec. III. We focused on the static structure factors at (π,π) and $(0,\pi)$ and performed the numerical scans over K/J_1 for various values of J_2/J_1. In agreement with the analytical predictions, the scans performed for small J_2/J_1 have shown that the antiferromagnetic (π,π) phase transforms into the canted spin configurations of Fig. 1(a), and the latter, in turn, undergoes a first-order transition into the orthogonal configuration of Fig. 1(c) under the further increase of K.

For J_2/J_1 close to $\frac{1}{2}$, the calculations of $S(\vec{q})$ and the susceptibilities of the columnar and staggered dimers allowed us to find, first, a transition from the (π,π) Néel phase to the dimerized phase presumably via a intermediate disordered state and, second, a transition between the two different dimerized states at some intermediate K. For large J_2/J_1, the numerical calculations detected that when K increases, the magnetically ordered $(0,\pi)$ phase transforms into the intermediate canted configuration, which, in turn, is substituted by the orthogonal one under the further increase of K.

While the general structure of the phase diagram emerging from the analytical and numerical approaches

turns out to be practically the same, the locations of various phase boundaries may differ significantly. Thus, the instability of the (π,π) phase occurs at lower values of K than predicted analytically. On the other hand, the region of the intermediate canted phase for large J_2 stretches up to much larger values of K than one might expect from the analysis of Sec. II. Also, the scan over K at $J_2/J_1=0.60$ did not find a broad region of the dimerized state in apparent contradiction with the phase diagram of Fig. 4. At least, the intermediate phase found for $J_2/J_1>\frac{1}{2}$ presumably has a more complicated structure than the simple canted configuration of Fig. 1(b), since the structure factor $S(\pi,\pi)$ increases with K instead of being almost a constant as would be the case if the canted phase would preserve the pure antiferromagnetic ordering along diagonals.

While some of the discrepancies seem to be attributed to the finite size of the clusters, we do not exclude that the actual phase diagram is asymmetric with respect to $J_2/J_1=\frac{1}{2}$. Specifically, one should require the upper boundary of the dimerized phase to move towards lower values of J_2/J_1 as K increases to reestablish the agreement with the numerical data. The required change in the location of the boundary line is most likely to be attributed to quantum fluctuations, not included in this approach, which was intended to search for the different magnetic phases but not for the precise location of the phase boundaries.

ACKNOWLEDGMENTS

We acknowledge useful conversations with S. Bacci, E. Dagotto, E. Fradkin, T. Jolicoeur, R. M. Martin, and M. Roger. The work by A.C. and E.G. was supported by NSF Grant No. STC-8809854 through the Science and Technology Center for Superconductivity at the University of Illinois at Urbana-Champaign.

*Permanent address: P. L. Kapitza Institute for Physical Problems, Moscow, U.S.S.R.

[1]See *Proceedings of the Los Alamos Symposium on High Temperature Superconductivity,* edited by K. S. Bedell, D. Coffey, D. E. Meltzer, D. Pines, and J. R. Schrieffer (Addison-Wesley, Reading, MA 1989).

[2]C. A. Balseiro, M. Avignon, A. G. Rojo, and B. Alascio, Phys. Rev. Lett. **62**, 2624 (1989), and references therein.

[3]S. L. Cooper *et al.*, Phys. Rev. B **42**, 10785 (1990); T. Thio *et al.*, *ibid.* **42**, 10800 (1990); Y. Ohta *et al.*, Phys. Rev. Lett. **66**, 1228 (1991).

[4]S. Bacci, E. Gaglinao, R. M. Martin, and J. Annett, Phys. Rev. B **44**, 7504 (1991). A value of $U=4.1$ eV has been derived numerically [E. Stechel and M. Hybertsen (private communication)] and shown to be consistent with x-ray absorption in $La_{2-x}Sr_xCuO_{4+\delta}$. C. T. Chen *et al.*, Phys. Rev. Lett. **66**, 104 (1991); M. Hybertsen, E. Stechel, M. Schluter, and D. Jennison, Phys. Rev. B **41**, 11068 (1990).

[5]E. Dagotto *et al.*, Phys. Rev. Lett. **67**, 1918 (1991).

[6]E. Dagotto *et al.* (unpublished).

[7]C. T. Chen *et al.*, Phys. Rev. Lett **66**, 104 (1991).

[8]A. H. MacDonald, S. M. Girvin, and D. Yoshioka, Phys. Rev. B **41**, 2565 (1990).

[9]V. J. Emery, Phys. Rev. Lett. **58**, 2794 (1987); J. Hirsch, *ibid.* **60**, 1668 (1988); A. K. McMahan, R. M. Martin, and S. Satpathy, Phys. Rev. B **38**, 6650 (1988); **42**, 6268 (1990); M. S. Hybertsen, M. Schluter, and N. E. Christensen *ibid.* **39**, 9028 (1989); J. F. Annett, R. M. Martin, A. K. McMahan, and S. Satpathy, *ibid.* **40**, 2620 (1989); see also Ohta (Ref. 3).

[10]M. Roger and J. M. Delrieu, Phys. Rev. B **39**, 2299 (1989).

[11]E. Gagliano *et al.*, Europhys. Lett. **12**, 259 (1990); H. J. Schmidt and Y. Kuramoto, Physica C **167**, 263 (1990).

[12]From small cluster calculations, it is hard to extract the value of J_3, but the estimates show that it is much smaller than J_2.

[13]S. Sugai *et al.*, Phys. Rev. B **42**, 1045 (1990).

[14]For $U/t=4$ (12), the ground-state energy of the Hubbard model calculated for 4×4 cluster differs from the ground-state energy of Eq. (1), with the exchange parameters given by $J_1=4t^2/U-24t^4/U^3$, $J_2=J_3=4t^4/U^3$, and $K=40t^4/U^3$, by 6% (0.06%).

[15]E. Dagotto and A. Moreo, Phys. Rev. Lett. **63**, 2148 (1989); A. Moreo, E. Dagotto, T. Jolicoeur, and J. Riera, Phys. Rev. B **42**, 6283 (1990).

[16]D. Poilblanc, E. Gagliano, S. Bacci, and E. Dagotto, Phys. Rev. B **43**, 10970 (1991); R. Singh and R. Narayanan, Phys. Rev. Lett. **65**, 1072 (1990).

[17]N. Read and S. Sachdev, Phys. Rev. Lett. **62**, 1694 (1989); **66**, 1773 (1991); S. Sachdev and R. N. Bhatt, Phys. Rev. B **41**, 9323 (1990).

[18]A. V. Chubukov and Th. Jolicoeur, Phys. Rev. B **44**, 12050 (1991).

[19]M. P. Gelfand, R. R. P. Singh, and D. A. Huse, Phys. Rev. B **40**, 10801 (1989); J. Stat. Phys. **59**, 1093 (1990); M. P. Gelfand, Phys. Rev. B **42**, 8206 (1990).

[20]See, for example, E. Manousakis, Rev. Mod. Phys. **63**, 1 (1990), and references therein.

[21]L. B. Ioffe and A. I. Larkin, Int. J. Mod. Phys. B **2**, 203 (1988); P. Chandra and B. Douçot, Phys. Rev. B **38**, 9335 (1988); T. Einarsson and H. Johannesson, *ibid.* **43**, 5867 (1991).

[22]M. Roger, J. M. Delrieu, and J. H. Hetherington, Rev. Mod. Phys. **55**, 1 (1983).

[23]H. Godfrin, R. R. Ruel, and D. D. Osheroff, Phys. Rev. Lett. **60**, 305 (1988).

[24]A. Chubukov, Phys. Rev. B **44**, 392 (1991).

[25]F. Mila, D. Poilblanc, and C. Bruder, Phys. Rev. B **43**, 7891 (1991).

[26]J. Villain, R. Bidaux, J. Carton, and R. Conte, J. Phys. (Paris) **41**, 1263 (1980).

[27]E. Shender, Zh. Eksp. Teor. Fiz. **83**, 326 (1982) [Sov. Phys.—JETP **56**, 178 (1982)]; P. Chandra and P. Coleman, Int. J. Mod. Phys. B **3**, 1729 (1989).

[28]A. V. Chubukov, Pis'ma Zh. Eksp. Teor. Fiz. **49**, 108 (1989) [JETP Lett. **49**, 129 (1989)]. A different bosonization technique which resembles the Schwinger boson approach referenced to dimerized states was proposed by Sachdev and Bhatt (Ref. 17).

[29]A. Chubukov, Phys. Rev. B **43**, 3337 (1991).

[30]E. Dagotto and A. Moreo, Phys. Rev. D **31**, 865 (1985); E. Gagliano, E. Dagotto, A. Moreo, and F. Alcaraz, Phys. Rev. B **34**, 1677 (1986).